

# Hubbard pair cluster in the external fields. Studies of the chemical potential

T. Balcerzak, K. Szałowski\*

*Department of Solid State Physics, Faculty of Physics and Applied Informatics,  
 University of Łódź, ulica Pomorska 149/153, 90-236 Łódź, Poland*

---

## Abstract

The chemical potential of the two-site Hubbard cluster (pair) embedded in the external electric and magnetic fields is studied by exact diagonalization of the Hamiltonian. The formalism of the grand canonical ensemble is adopted. The influence of temperature, Hubbard on-site Coulombic energy  $U$  and electron concentration on the chemical potential is investigated and illustrated in figures. In particular, a discontinuous behaviour of the chemical potential (or electron concentration) in the ground state is discussed.

**Keywords:** Hubbard model, dimer, pair cluster, chemical potential, exact diagonalization, grand canonical ensemble

**PACS:** 67.10.Fj, 71.10.-w, 73.22.-f, 75.10.Lp

---

## 1. Introduction

The Hubbard model [1–4] has been comprehensively studied over the last decades [5–63]. Its applicability involves, for example, the description of metal-insulator transition, ferromagnetism of itinerant electrons, studies of high-temperature superconductors, optical lattices and graphene magnetism. In spite of intensive efforts, so far the exact solution has been obtained only in 1D case [13, 46], including the solution for the case of Hubbard model in external magnetic field [47, 48]. As far as 2D systems are concerned, the Mermin-Wagner theorem about the absence of magnetic ordering for non-zero temperatures is worthy of mention [51, 52, 59]. In turn, for the systems being in the ground state, the Lieb theorems [12] have been formulated.

Regarding implications for the magnetism, it has been shown that for the Hubbard parameter  $U \rightarrow \infty$  (and  $U > 0$ ) the so-called  $t - J$  model [57] can be derived, which, for half-filling of the band is equivalent to the model of isotropic Heisenberg antiferromagnet [1, 58]. In turn, for  $U \rightarrow \infty$  (and  $U < 0$ ) the Hubbard Hamiltonian becomes equivalent to that of XXZ model [7, 60].

Parallel to the exact (or rigorous) results mentioned above, the approximate methods, both analytic and numerical, have been developed with different amount of success. Among them the

---

\*Corresponding author. Email address: kszalowski@uni.lodz.pl

Email addresses: t\_balcerzak@uni.lodz.pl (T. Balcerzak), kszalowski@uni.lodz.pl (K. Szałowski)

Quantum Monte Carlo (QMC) methods [18, 42] and Dynamical Cluster Approximation (DCA) [20] deserve particular attention.

The possible extensions of the domain where the exact solutions can be found for the model include the zero-dimensional, cluster systems (see for example [22, 23]) as well as clusters embedded in the environment of localized spins [24–27]. It is worthy to mention that the studies of such geometrically confined, cluster systems are important from the point of view of nanophysics and nanotechnology. In particular, it has been shown in [22, 23] that for some small number of electrons the analytic solutions can be obtained in addition to the numerical calculations. The magnetic field has been taken into account in [22], however, the influence of the external electric field on the cluster properties has not been studied there.

Motivated by such a possibility, we undertake the exact study of the Hubbard simplest cluster, namely the pair (or dimer), embedded simultaneously in the external magnetic and electric fields. We note that such system has already attracted some attention [28–35]. Also the effect of the electric field on the properties of the Hubbard model was studied [36, 37]. However, the simultaneous influence of both external electric and magnetic field on the Hubbard dimer was not discussed. It can be mentioned that the usefulness of such model can be related to hydrogen molecule [38] or several layered organic strongly correlated compounds [39]. We perform analytic diagonalization of the pair Hamiltonian and proceed using the formalism of the grand canonical ensemble, where the mean number of electrons in the system can vary and results from thermodynamic equilibrium conditions. This enables to obtain the grand thermodynamic potential as well as the average values of relevant operators. However, the statistical-thermodynamic calculations are possible provided the chemical potential is known. Therefore, as the first stage, we found it particularly important to calculate accurately the chemical potential for such an open system, interacting with the environment.

In this paper we concentrate exclusively on the comprehensive calculations of the chemical potential for the Hubbard pair, especially we study its behaviour in the external magnetic and electric fields, in a wide range of temperatures. In particular, for low temperature range the quantum changes of the chemical potential are investigated. The influence of Hubbard energy  $U$  on the chemical potential is also studied.

In the next section the outline of the theoretical method will be presented. In the successive section the numerical results will be illustrated in figures and their discussion will be given.

## 2. Theoretical model

The Hubbard Hamiltonian for a pair of atoms ( $a, b$ ) in the external fields is assumed in the form of:

$$\begin{aligned} \mathcal{H}_{a,b} = & -t \sum_{\sigma=\uparrow,\downarrow} (c_{a,\sigma}^+ c_{b,\sigma} + c_{b,\sigma}^+ c_{a,\sigma}) + U (n_{a,\uparrow} n_{a,\downarrow} + n_{b,\uparrow} n_{b,\downarrow}) \\ & - H (S_a^z + S_b^z) - V (n_a - n_b), \end{aligned} \quad (1)$$

where  $t > 0$  is the hopping integral and  $U \geq 0$  is on-site Coulomb repulsion energy. The symbol  $H = -g\mu_B H^z$  introduces an external magnetic field  $H^z$ , with  $g$  being a gyromagnetic factor for the

electron and  $\mu_B$  denoting the Bohr magneton. Moreover,  $V = E|e|d/2$  denotes the electrostatic potential of uniform electric field  $E$  oriented along the pair, with  $d$  being the interatomic distance, whereas  $e$  is the electron charge. For the sake of simplicity, we will assume that the hopping integral is not dependent on the external fields. In Eq.(1)  $c_{\gamma,\sigma}^+$  and  $c_{\gamma,\sigma}$  are the electron creation and annihilation operators, respectively, and  $\sigma$  denotes the spin state. The matrix form of the creation and annihilation operators has been derived in Appendix A. Occupation number operators  $n_\gamma$  for site  $\gamma = a, b$ , are expressed by these creation and annihilation operators:  $n_\gamma = \sum_\sigma n_{\gamma,\sigma} = \sum_\sigma c_{\gamma,\sigma}^+ c_{\gamma,\sigma}$ , whereas the resulting  $z$ -components of the spins,  $S_\gamma^z$ , are:  $S_\gamma^z = (n_{\gamma,\uparrow} - n_{\gamma,\downarrow})/2$ .

As shown in the Appendix B, the pair Hamiltonian (1) can be represented by  $16 \times 16$  matrix. The exact analytic diagonalization of the Hamiltonian has been performed (see Appendix B). Treating the pair-cluster as an open electronic system, the grand thermodynamic potential  $\Omega_{a,b}$  can be obtained from the general formula:

$$\Omega_{a,b} = -k_B T \ln \mathcal{Z}_{a,b} = -k_B T \ln \{ \text{Tr}_{a,b} \exp[-\beta (\mathcal{H}_{a,b} - \mu (n_a + n_b))] \}, \quad (2)$$

where  $\mathcal{Z}_{a,b}$  is the grand partition function and  $\mu$  is the chemical potential. The knowledge of  $\Omega_{a,b}$  enables the self-consistent calculations of all thermodynamic properties.

After diagonalization, the thermodynamic mean value of any operator  $\hat{O}$  can be calculated as:

$$\langle \hat{O} \rangle = \text{Tr}_{a,b} [\hat{O} \hat{\rho}_{a,b}], \quad (3)$$

where  $\hat{\rho}_{a,b}$  is the statistical operator for the grand canonical ensemble:

$$\hat{\rho}_{a,b} = \frac{1}{\mathcal{Z}_{a,b}} \exp[-\beta (\mathcal{H}_{a,b} - \mu (n_a + n_b))]. \quad (4)$$

The chemical potential  $\mu$  of the electrons fulfils the relationship:

$$\langle n_a \rangle + \langle n_b \rangle = - \left( \frac{\partial \Omega}{\partial \mu} \right)_{T,H,E} \quad (5)$$

where  $\langle n_a \rangle$  and  $\langle n_b \rangle$  are the thermodynamic mean values of the total occupation number operators for  $a$  and  $b$  sites, respectively. These averages are parametrized by  $\mu$  and can be calculated according to the general formula (3). The partial derivative in Eq.(5) is performed at constant temperature  $T$  and external fields  $H$  and  $E$ . In order to find  $\mu$  we define the parameter  $x$  denoting the mean number of electrons per lattice site, namely:

$$x = (\langle n_a \rangle + \langle n_b \rangle) / 2 \quad (6)$$

Thus, from the relationship (6) the chemical potential  $\mu$  can be found as a function of  $T$ ,  $H$ ,  $E$  and  $x$ . For a pair of sites,  $x$  can take values from 0 to 2, since the system can house up to 4 electrons.

The results of numerical calculations performed in the framework of the above formalism are presented in the next section.

### 3. Numerical results and discussion

The numerical calculations have been performed on the basis of analytic solution as presented in the theoretical Section. Independently, in order to check analytic formulas, the numerical diagonalization of the pair Hamiltonian has been made using Mathematica software [64]. The excellent agreement for both methods has been found. The chemical potential has been calculated in a wide range of magnetic and electric fields, for arbitrary temperature, and in a full range of electron concentration  $0 \leq x \leq 2$ . For the calculations in the electric field, the external potential  $V = V_a = -V_b = E|e|d/2$  has been selected.

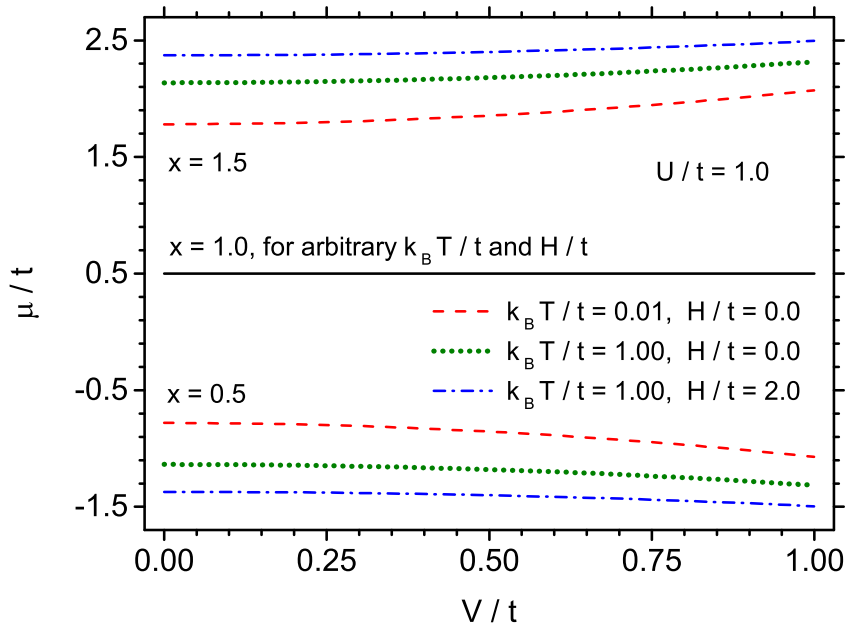


Figure 1: Chemical potential  $\mu/t$  vs. electric field potential  $V/t$  ( $V = E|e|d/2$ ), for  $U/t = 1$  and different electron concentrations  $x$  per atom. Two different temperatures:  $k_B T/t = 0.01$  and  $k_B T/t = 1$ , as well as two magnetic fields:  $H/t = 0$  or  $H/t = 2$  are chosen.

In Fig. 1 the dimensionless chemical potential  $\mu/t$  is shown vs. normalized electric field  $E|e|d/(2t)$ , for two different temperatures  $k_B T/t=0.01$  and  $k_B T/t=1$ . For higher temperature the effect of magnetic field with the value  $H/t=2$  is shown additionally. The curves are plotted for the electron concentrations  $x=0.5$ , 1 and 1.5. The Hubbard  $U$  parameter is set to  $U/t = 1$ . At first it can be noted that for  $x = 1$  (i.e. for half-filling) the chemical potential is equal to  $U/2$  and it does not depend on the temperature and the external fields. This is in agreement with our knowledge about the Hubbard model for infinite system. Moreover, for  $x \neq 1$  the results are symmetric with respect to that for  $x = 1$ . For instance, it can be seen that for  $x = 1.5$ , by increasing temperature the chemical potential also increases, whereas for  $x = 0.5$  a symmetric decrease of  $\mu/t$  is present.

The dependence of  $\mu/t$  on the electric field is rather weak in this figure and much smaller than on the magnetic field. For instance, for  $k_B T/t=1$  a remarkable splitting of two curves: for  $H/t=0$  and  $H/t=2$  can be noticed. The increasing electric field  $E$  makes a slow increase of the chemical potential for  $x > 1$ , whereas for  $x < 1$  a symmetric slow decrease of  $\mu/t$  is observed.

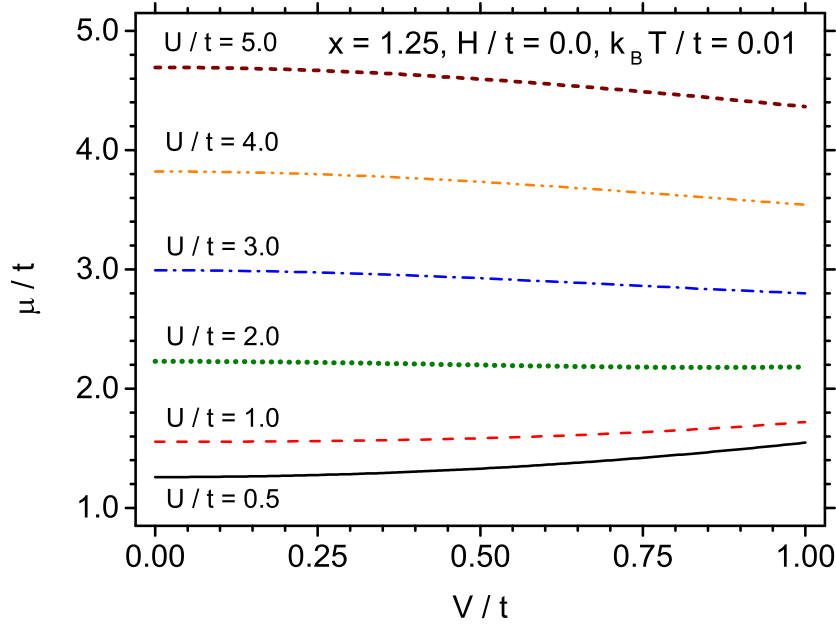


Figure 2: Chemical potential  $\mu/t$  vs. electric field potential  $V/t$  ( $V = E|e|d/2$ ), for electron concentrations  $x = 1.25$  per atom (weak electron doping) and different  $U/t$ . Temperature amounts to  $k_B T/t = 0.01$  and the magnetic field is absent.

The dependence of the chemical potential on the electric field potential, for various Hubbard parameters  $U$  is shown in Fig. 2. In this figure the mean electron concentration is chosen as  $x = 1.25$ , which goes beyond the half-filling, towards small electron doping. The temperature  $k_B T/t = 0.01$  is close to the ground state and the magnetic field is equal to zero. It is seen that the chemical potential  $\mu$  strongly depends on the parameter  $U$ , and increases with an increase of  $U$ . At the same time, a slowly increasing function of  $\mu$  vs.  $V$ , seen for small  $U$ , converts into a decreasing one when  $U$  increases.

A relationship between  $\mu$  and the electric field potential  $V$  for different magnetic fields is illustrated in Fig. 3. In this case  $U/t = 2.5$ , whereas the parameter  $x$  and temperature are the same as in Fig. 2. It is seen that for higher magnetic fields the curves are not monotonous, and have a sharp minimum if the electric field potential  $V$  is large enough. On closer inspection of the magnetization, the minima presented for  $H/t = 2$  and  $H/t = 3$  are connected with ferrimagnetic phase

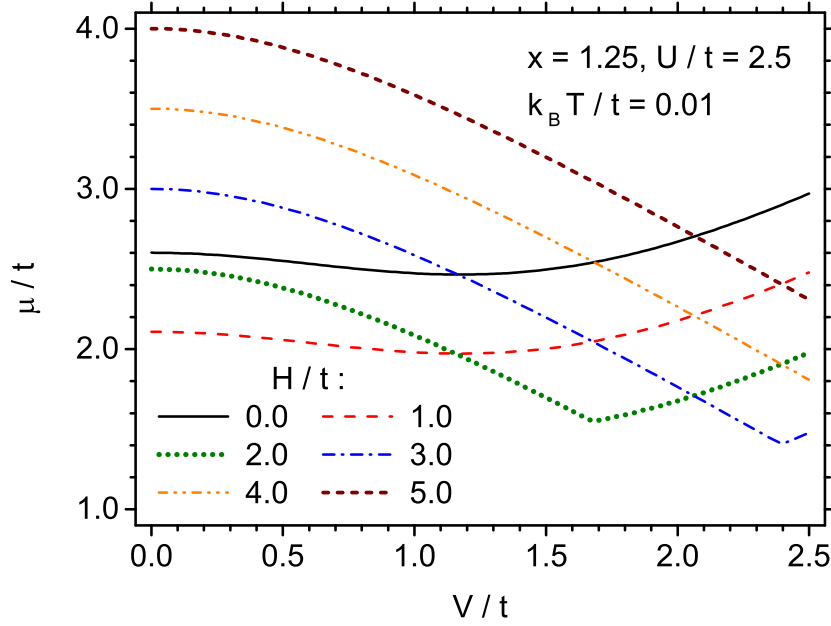


Figure 3: Chemical potential  $\mu/t$  vs. electric field potential  $V/t$  ( $V = E|e|d/2$ ), for electron concentrations  $x = 1.25$  per atom and different magnetic field  $H/t$ . Temperature amounts to  $k_B T/t = 0.01$  and the Hubbard parameter is  $U/t = 2.5$ .

transitions from saturated phase (with  $\langle S_a^z + S_a^z \rangle = 0.75$  for low  $V$ ) to the phase with lower total magnetization ( $\langle S_a^z + S_a^z \rangle = 0.25$ ), when  $V$  increases. The analogous minima occur also for larger fields  $H/t$ , however, they are not seen in the frame of this figure.

In Fig. 4 the chemical potential  $\mu/t$  is illustrated vs. dimensionless temperature  $k_B T/t$  for various electron concentration  $x$ . The electric and magnetic fields are absent and the  $U$  parameter is equal to  $U/t = 1$ . The curves for different  $x$  are distributed symmetrically with respect to the curve for  $x = 1$ . For the electron concentration  $x$  approaching the value  $x = 1$  a non-monotonous behaviour of the curves is observed. On the other hand, for  $x$  tending to 2 the chemical potential is an increasing function of temperature, whereas for  $x$  tending to 0 it monotonously decreases.

In the next figure (Fig. 5) the chemical potential is presented as a function of the external magnetic field  $H/t$ , for different electron concentration  $x$ . The remaining parameters are:  $E=0$  and  $U/t = 1$ . Also in this case the symmetry of the curves with respect to the curve for  $x = 1$  is seen, and non-monotonous behaviour when  $x$  approaches the value  $x = 1$  can be noticed. From the Figs. 4 and 5 it is seen that for  $x = 1$  the chemical potential does not depend on the temperature and magnetic field, in accordance with Fig. 1.

The calculation of  $\mu/t$  vs. electron concentration  $x$  is illustrated in Fig. 6 for different Hubbard

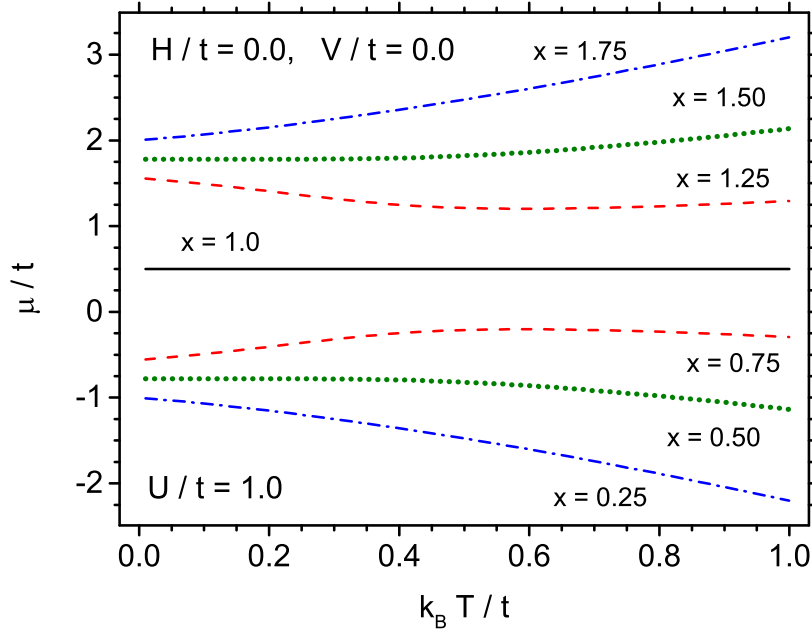


Figure 4: Chemical potential  $\mu/t$  vs. temperature  $k_B T/t$ , for  $U/t = 1$  and different electron concentrations  $x$  per atom. The magnetic and electric fields are set to zero.

energies  $U$ , at constant temperature  $k_B T/t=0.5$ . In Fig. 6 the external fields are equal to zero. All the curves are monotonous vs.  $x$ , with the strongest dependency for  $x \rightarrow 0$  and  $x \rightarrow 2$ . The fact that  $\partial\mu/\partial x > 0$  is important from the thermodynamic point of view, since it proves the chemical stability of the system. For  $x = 1$  (i.e., for half-filling) the chemical potential fulfils the relation  $\mu = U/2$ . It can also be noted that for small  $x$  the chemical potential is negative and it becomes independent on  $U$ .

In Fig. 7 the chemical potential  $\mu/t$  vs. electron concentration  $x$  is presented, for different electric field potentials  $V/t$ . The magnetic field is also present in this case, with the constant value  $H/t=1$ , while  $U/t=1$ . Since the temperature  $k_B T/t = 0$ , the chemical potential becomes quantized and is represented by the step-wise function, which shows the steps when the total mean number of electrons in the system,  $2x$ , amounts to 0, 1, 2, 3 and 4. The influence of electric field potential is evident, manifesting itself by an increasing height of the steps, whereas the concentrations  $x$  at discontinuity points remains the same. The effect of quantization has not been seen in the previous figure (Fig. 6), because the temperature was too high there.

In order to demonstrate the temperature effect on quantization, the dependency of  $\mu/t$  on the electron concentration  $x$  is plotted in Fig. 8 for two very different temperatures:  $k_B T/t=0$  (i.e., in the ground state) and  $k_B T/t=1$ . In addition, absence of the magnetic field, or its presence with

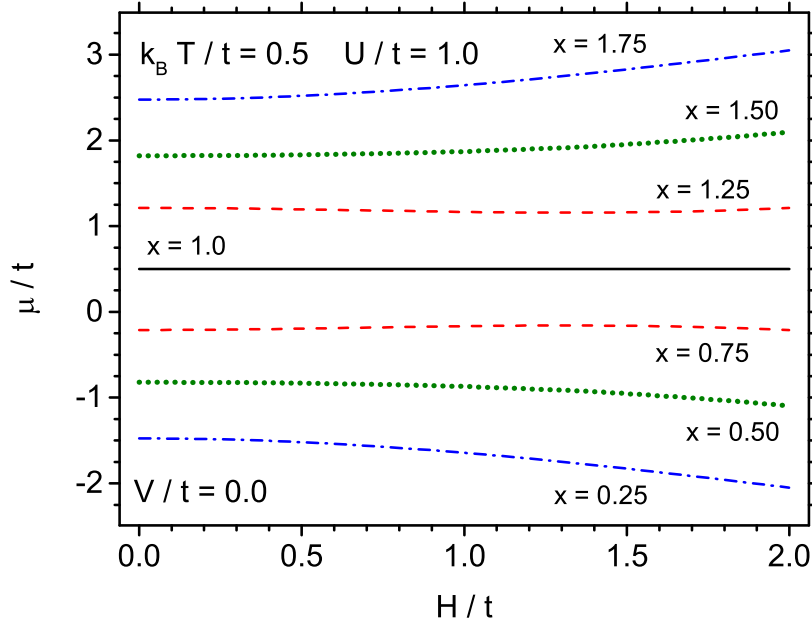


Figure 5: Chemical potential  $\mu/t$  vs. magnetic field  $H/t$ , for  $U/t = 1$  and different electron concentrations  $x$  per atom. Temperature is  $k_B T/t = 0.5$  and the electric field is set to zero.

the value  $H/t = 2$ , is taken into account, whereas  $E = 0$  and  $U/t=3$ . Again, it is seen that in the ground state the chemical potential changes discontinuously when the concentrations take the values:  $x = 0, 0.5, 1, 1.5$  and  $2$ . As expected, such a quantum behaviour is not present in the high temperature region, where the strong thermal fluctuations are present. In the ground state, the influence of the magnetic field is seen only in the regions  $0 \leq x \leq 0.5$  and  $1.5 \leq x \leq 2$ , whereas no effect on  $\mu$  in the region of  $0.5 < x < 1.5$  is noticed. On the other hand, for relatively large temperature,  $k_B T/t=1$ , the magnetic field influences the chemical potential practically in the whole region of  $x$ , with the exclusion of  $x = 1$  where  $\mu/t = 1.5$ .

In Fig. 9 the chemical potential  $\mu/t$  is plotted as a function of  $U/t$ , for different concentrations  $x$  and constant temperature  $k_B T/t=0.5$ . The absence or presence of the magnetic field with rather high value,  $H/t = 3$ , is taken into account, whereas the electric field is set to  $E = 0$ . Only for  $x = 1$  the ideal linear behaviour is observed, which is in accordance with  $\mu = U/2$ . In general,  $\mu$  is an increasing function of  $U$ , however, for small  $x$  the chemical potential becomes only weakly dependent on  $U$ , which is in accordance with Fig. 6. The magnetic field makes the curves more flat for  $x < 1$  and more steep for  $x > 1$ , with no influence observed for  $x = 1$ . Again, the curves are symmetric with respect to the case of  $x = 1$ . An increase of the Hubbard energy  $U$ , which stands for on-site Coulomb repulsion, means that also increasing chemical potential is needed for the electron to be adsorbed by the open system. A significant increase of  $\mu$  is observed when both



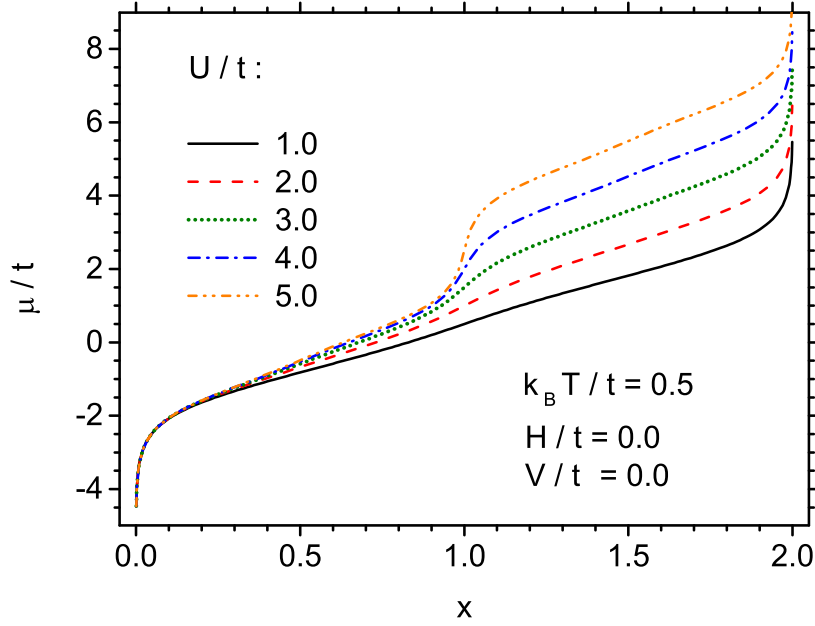


Figure 6: Chemical potential  $\mu/t$  as a function of electron concentration  $x$  per atom, for different Hubbard parameters  $U/t$ . Temperature is  $k_B T/t = 0.5$  and the magnetic and electric fields are set to zero.

$U$  and  $x$  are large.

Treating chemical potential as a variable, the resulting electron concentration  $x$  is plotted in Fig. 10. In such approach the chemical potential can be understood as an uniform external potential acting on the pair of atoms, whereas the electrons can be freely exchanged between the pair-cluster and its environment. In order to preserve this condition, the electric field is set to  $E = 0$ . Resulting mean number of electrons per atom (i.e., concentration  $x$ ) shows a step-wise behaviour at low temperatures, seen already at  $k_B T/t=0.1$ , and, in particular, in the ground state, when  $k_B T/t=0$ . After applying the external magnetic field with the value  $H/t = 1$ , the ranges of plateaus (horizontal parts of concentration  $x$ , representing the intervals of charge stability) are changed in comparison with the case of  $H = 0$ . This is an effect of energy competition between the Coulombic repulsion for on-site electrons and the magnetic Zeeman term. It should be noticed that the external magnetic field is not able to change the height of the steps, which occur for  $x=0, 0.5, 1, 1.5$ , and  $2$ , i.e., for the same values as in Fig. 8. One should also notice that the energy  $U$  in Fig. 10,  $U/t=1$ , differs from that in Fig. 8. As it could be expected, the common point for all curves presented in Fig. 10 lies at  $(\mu/t = 0.5, x = 1)$ .

In the next figure (Fig. 11) the grand potential,  $\Omega/t$ , is presented vs. chemical potential  $\mu/t$ , in the absence of external fields but for different temperatures. The Hubbard energy  $U$  amounts to

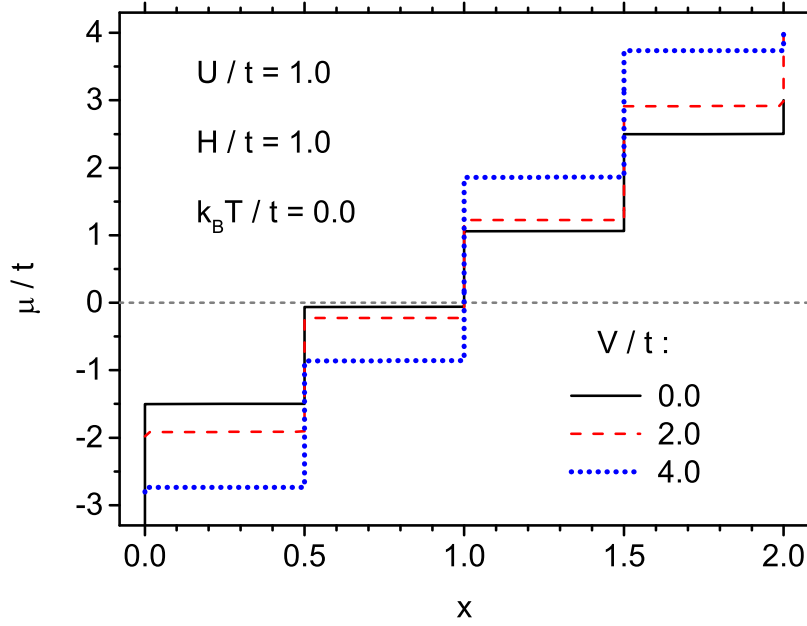


Figure 7: Chemical potential  $\mu/t$  as a function of electron concentration  $x$  per atom, for different electric field potentials  $V/t$ . Temperature is  $k_B T/t = 0$ , whereas the magnetic field is set to  $H/t=1$  and the Hubbard parameter  $U/t=1$ .

$U/t = 1$ , thus, in the ground state, the result can be related to the corresponding  $x$ -curve in Fig. 10. It can be seen that for  $k_B T/t=0$  the grand potential has the kinks at  $\mu/t = -1, -0.56, 1.56$ , and  $2$ , i.e., at the same discontinuity points as  $x$  in Fig. 10. We can identify these discontinuity points as the limits of the intervals where the integer number of electrons is present in the Hubbard pair, whereas the system is in the ground state. Within these intervals the grand potential is presented by the straight lines, and its derivative, i.e., the number of electrons (see Eq. 5), is constant. By increasing the temperature, the grand potential transforms into the smooth curve, which monotonically decreases with increase of  $\mu$ . We also see that for constant  $\mu$ , the increase of temperature involves always a decrease of  $\Omega$ . Hence, it can be concluded that the entropy,  $S = -(\partial\Omega/\partial T)_\mu$ , will be positive for all  $\mu$  and  $T$ .

Quantum behaviour of the electron concentration for low temperatures is also illustrated in Fig. 12. In this diagram the isolines representing constant chemical potentials,  $\mu/t$ , are plotted in the coordinates  $x$  and  $k_B T/t$ . The isolines are separated by  $|\Delta\mu|/t = 0.5$ . The external magnetic field is set to zero, whereas  $V/t = 1$  and the energy  $U$  is  $U/t = 1$ . It can be seen that for  $T = 0$  only five values of electron concentration are allowed, which are distributed symmetrically around  $x = 1$ , and the  $\mu$  values can be divided into five groups. These groups correspond to five regions of constant electron concentrations, as discussed in Fig. 11 for the ground state. By increasing temperature, the discrete values of  $x$  are transformed into the continuous spectrum extending over

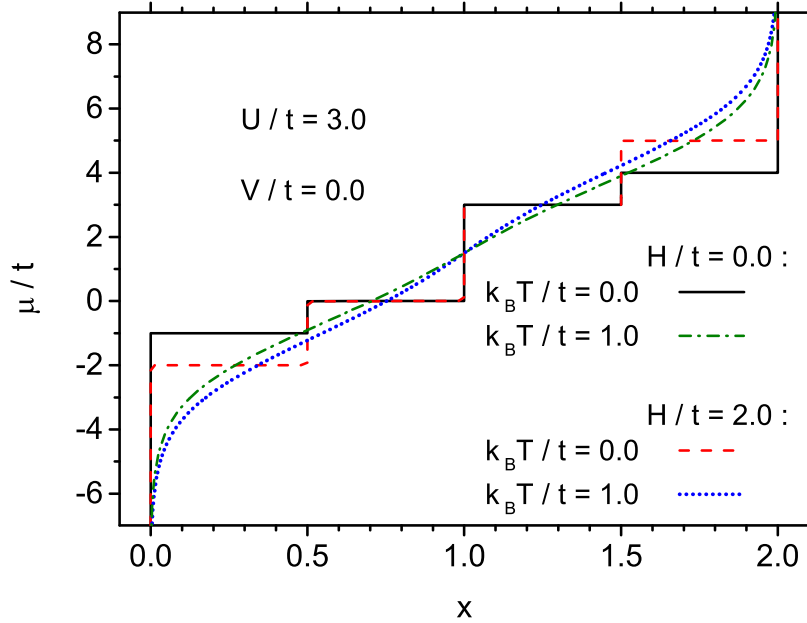


Figure 8: Chemical potential  $\mu/t$  vs. electron concentrations  $x$  per atom, for  $U/t = 3$  and two different temperatures:  $k_B T/t = 0$  and  $k_B T/t = 1$ . Two magnetic fields are chosen:  $H/t = 0$  and  $H/t = 2$ , whereas the electric field is set to zero.

arbitrary  $\mu$  value. Similarly to the ground state, the spectrum remains symmetric around  $(x = 1, \mu/t = 0.5)$  for all the temperatures.

In Fig. 13, the isolines representing the constant magnetic fields,  $H/t$ , which all correspond to the constant chemical potential with the value  $\mu/t = -1$ , are plotted in the coordinates  $x$  and  $k_B T/t$ . The electric field is assumed as  $V/t=0.5$  and the energy  $U$  is set to  $U/t = 1$ . Again, quantum behaviour of the electron concentration  $x$  in the ground state is observed. The curves in Fig. 13 presents an evolution of the constant chemical potential curve (with the value  $\mu/t = -1$ ) under the influence of the magnetic field. In particular, it is demonstrated that for high temperatures the increase of the magnetic field causes a continuous increase of the electron concentration  $x$ . However, for small  $T$ , the process of increasing  $x$  becomes quantized, and the highest electron concentration, which can be reached when  $H$  increases, is  $x = 1$ . It can also be noticed that each curve presented in previous Fig. 12, and described by the constant parameters  $\mu$ ,  $U$  and  $H = 0$ , can be studied in the external magnetic field analogously to the present case (Fig. 13).

In the last figure (Fig. 14) the isolines of constant electric field potential are presented, in the coordinates  $x$  and  $k_B T/t$ . The isolines correspond to  $U/t=5$  and constant chemical potential  $\mu/t = 1$ , whereas the magnetic field is set to zero. It is seen that these isolines can be classified into two groups, due to quantization of electron concentration for  $T = 0$ . Namely, for such a

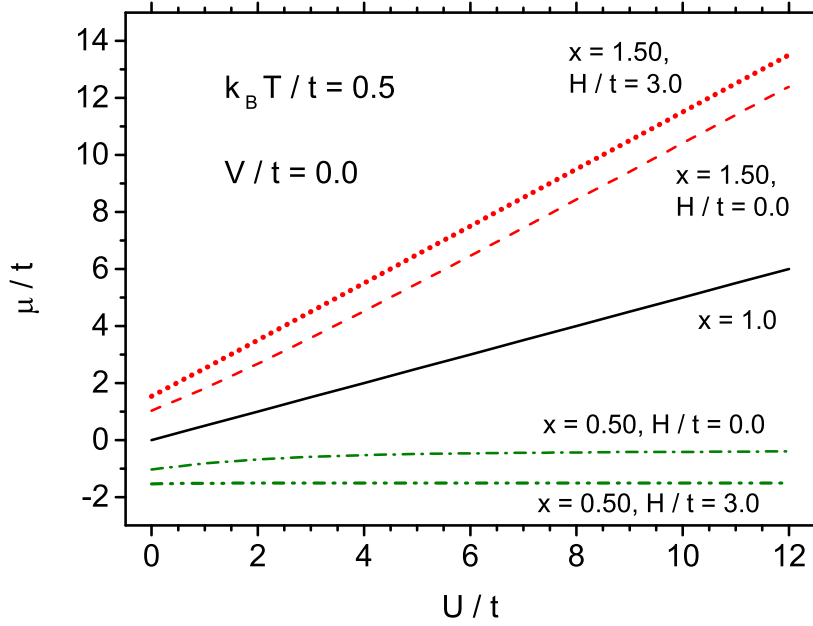


Figure 9: Chemical potential  $\mu/t$  vs. Hubbard  $U/t$ -parameter, for  $k_B T/t = 0.5$  and different electron concentrations  $x$  per atom. Two magnetic fields are chosen:  $H/t = 0$  and  $H/t = 3$ , whereas the electric field is set to zero.

set of parameters, only one or two electrons can exist in the ground state (i.e.,  $2x=1$  or  $2x=2$ ). The same quantization was observed in the previous figure (Fig. 13). Again, for higher temperatures the spectrum becomes continuous, and, at the same time, the range of allowed  $x$  is narrowing.

#### 4. Summary and conclusion

In the paper we presented some selected results of exact calculations of the chemical potential for the Hubbard pair-cluster embedded in the external fields. The Hubbard pair is treated as an open system, where the mean number of electrons results from thermodynamic equilibrium. At first, we found that the dependence of  $\mu$  on the small electric field, when the external potential is applied asymmetrically to both atoms, is weaker than the dependence on the magnetic field (Fig. 1). However, in a wider range of  $V/t$  the influence of electric field is remarkable (Figs. 3, 7, 14). The influence of Hubbard  $U$  repulsion parameter has also been taken into account. In particular, for low temperatures the step-wise changes of the electron concentration (or, equivalently, chemical potential) are discussed.

It should be noticed that the curves representing the chemical potential are symmetric with respect to the half-filling case ( $x=1$ ,  $\mu = U/2$ ) due to a particle-hole symmetry. In particular, the consequences of this symmetry is seen in Figs. 1, 4, 6 - 10 and 12.

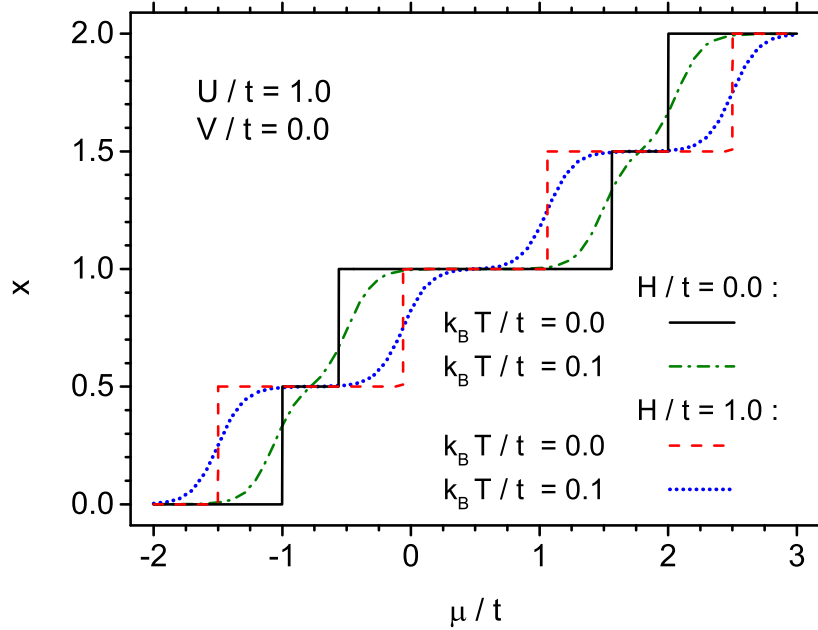


Figure 10: A step-wise behaviour of electron concentration  $x$  per atom vs. chemical potential  $\mu/t$ , for  $U/t = 1$ . Different curves correspond to two chosen temperatures:  $k_B T/t = 0$  and  $k_B T/t = 1$ , as well as two magnetic fields:  $H/t = 0$  and  $H/t = 1$ . The electric field is set to zero.

The calculations of the chemical potential, which may be performed over a wide range of parameters simultaneously taking into account the electric and magnetic fields, are of primary importance for further statistical-thermodynamic studies of the system in question. According to the theoretical background given in this paper, further investigations of open systems will be aimed at the exact calculations of all thermodynamic properties which can be obtained from the knowledge of the grand partition function. For instance, various correlation functions, mean energy, as well as all magnetic and electric properties can be calculated (in preparation). In particular, the thermodynamic response functions, such as the magnetic or electric susceptibilities, can be studied within the method. Such investigations should broaden our knowledge about the physics of small clusters.

## Appendix A. Construction of annihilation and creation operators

On the basis of Pauli matrices:

$$\sigma_x = \begin{pmatrix} 0 & 1 \\ 1 & 0 \end{pmatrix}, \quad \sigma_y = \begin{pmatrix} 0 & -i \\ i & 0 \end{pmatrix}, \quad \sigma_z = \begin{pmatrix} 1 & 0 \\ 0 & -1 \end{pmatrix}, \quad \text{and} \quad I = \begin{pmatrix} 1 & 0 \\ 0 & 1 \end{pmatrix} \quad (\text{A.1})$$

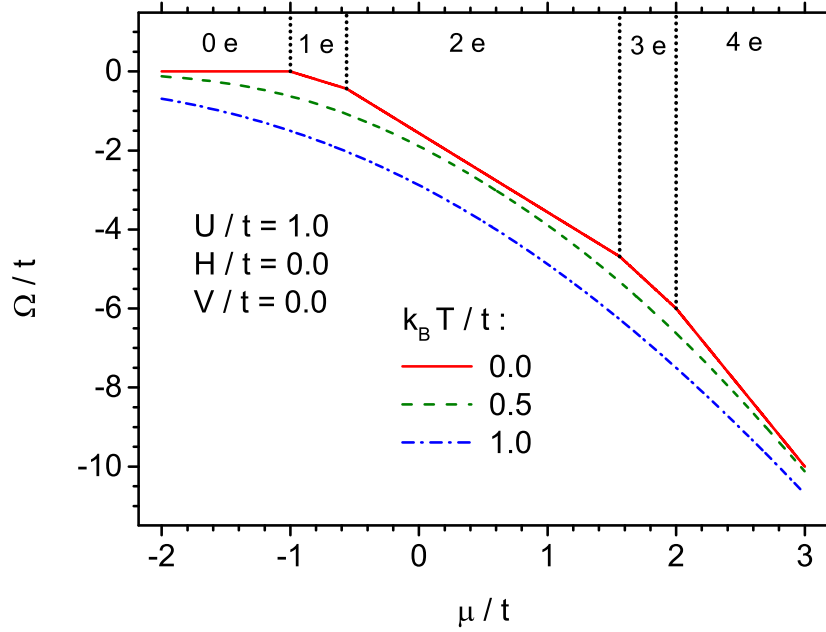


Figure 11: Grand potential  $\Omega/t$  as a function of the chemical potential  $\mu/t$ , for  $U/t = 1$  and three different temperatures. The magnetic and electric fields are set to zero.

the spin deviation operators are presented as follows:

$$\alpha = \frac{1}{2}(\sigma_x + i\sigma_y) = \begin{pmatrix} 0 & 1 \\ 0 & 0 \end{pmatrix}, \quad \alpha^+ = \frac{1}{2}(\sigma_x - i\sigma_y) = \begin{pmatrix} 0 & 0 \\ 1 & 0 \end{pmatrix}, \quad \text{and} \quad \beta = \sigma_z. \quad (\text{A.2})$$

We define single-particle auxiliary operators for the electron which can occupy 4 possible states ( $\gamma = a, b; \sigma = \uparrow, \downarrow$ ) [65]:

$$\begin{aligned} \alpha_1 &= \alpha \otimes I \otimes I \otimes I, & \beta_1 &= \beta \otimes I \otimes I \otimes I \\ \alpha_2 &= I \otimes \alpha \otimes I \otimes I, & \beta_2 &= I \otimes \beta \otimes I \otimes I \\ \alpha_3 &= I \otimes I \otimes \alpha \otimes I, & \beta_3 &= I \otimes I \otimes \beta \otimes I \\ \alpha_4 &= I \otimes I \otimes I \otimes \alpha, & \beta_4 &= I \otimes I \otimes I \otimes \beta, \end{aligned} \quad (\text{A.3})$$

where  $\otimes$  stands for the matrix outer product. Then, the annihilation operators in these 4 states are obtained by the ordinary matrix multiplication of the auxiliary operators:

$$\begin{aligned} c_1 &= \alpha_1 \\ c_2 &= \alpha_2 \beta_1 \\ c_3 &= \alpha_3 \beta_1 \beta_2 \\ c_4 &= \alpha_4 \beta_1 \beta_2 \beta_3. \end{aligned} \quad (\text{A.4})$$

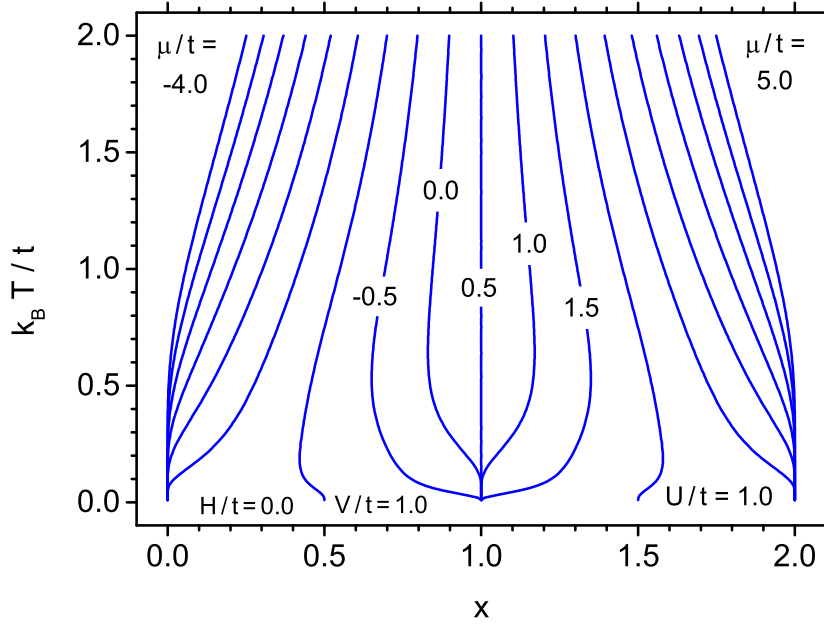


Figure 12: Isolines presenting the constant chemical potentials  $\mu/t$ , in the coordinates  $x$  (electron concentration per atom) and  $k_B T/t$  (temperature). The curves are separated by  $|\Delta\mu|/t = 0.5$ . The magnetic field is set to zero, whereas the electric field potential is  $V/t = 1$  and  $U/t = 1$ .

The numbering of states can be chosen as follows:

$$c_{a,\downarrow} = c_1, \quad c_{a,\uparrow} = c_2, \quad c_{b,\downarrow} = c_3, \quad c_{b,\uparrow} = c_4. \quad (\text{A.5})$$

The operators  $c_{a,\downarrow}$ ,  $c_{a,\uparrow}$ ,  $c_{b,\downarrow}$  and  $c_{b,\uparrow}$  are represented by  $16 \times 16$  sparse matrices with real elements. The only non-zero elements of these matrices are the following:

$c_{a,\downarrow}$ :

$$\begin{aligned} c_{a,\downarrow}[9, 1] &= c_{a,\downarrow}[10, 2] = c_{a,\downarrow}[11, 3] = c_{a,\downarrow}[12, 4] = \\ &= c_{a,\downarrow}[13, 5] = c_{a,\downarrow}[14, 6] = c_{a,\downarrow}[15, 7] = c_{a,\downarrow}[16, 8] = 1; \end{aligned} \quad (\text{A.6})$$

$c_{a,\uparrow}$ :

$$\begin{aligned} c_{a,\uparrow}[5, 1] &= c_{a,\uparrow}[6, 2] = c_{a,\uparrow}[7, 3] = c_{a,\uparrow}[8, 4] = 1, \\ c_{a,\uparrow}[13, 9] &= c_{a,\uparrow}[14, 10] = c_{a,\uparrow}[15, 11] = c_{a,\uparrow}[16, 12] = -1; \end{aligned} \quad (\text{A.7})$$

$c_{b,\downarrow}$ :

$$\begin{aligned} c_{b,\downarrow}[3, 1] &= c_{b,\downarrow}[4, 2] = c_{b,\downarrow}[15, 13] = c_{b,\downarrow}[16, 14] = 1, \\ c_{b,\downarrow}[7, 5] &= c_{b,\downarrow}[8, 6] = c_{b,\downarrow}[11, 9] = c_{b,\downarrow}[12, 10] = -1; \end{aligned} \quad (\text{A.8})$$

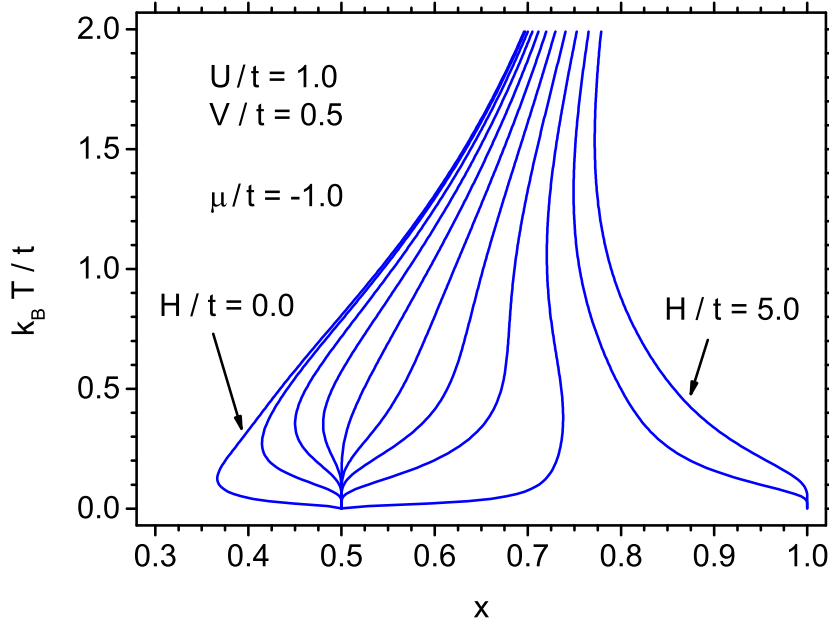


Figure 13: Isolines presenting constant magnetic fields  $H/t$ , in the coordinates  $x$  (electron concentration per atom) and  $k_B T/t$  (temperature). The curves are separated by  $|\Delta H|/t = 0.5$ . All curves correspond to the constant chemical potential  $\mu/t = -1$  and  $U/t = 1$ . The electric field potential is set to  $V/t = 0.5$ .

$c_{b,\uparrow}$ :

$$\begin{aligned} c_{b,\uparrow} [2, 1] &= c_{b,\uparrow} [8, 7] = c_{b,\uparrow} [12, 11] = c_{b,\uparrow} [14, 13] = 1, \\ c_{b,\uparrow} [4, 3] &= c_{b,\uparrow} [6, 5] = c_{b,\uparrow} [10, 9] = c_{b,\uparrow} [16, 15] = -1. \end{aligned} \quad (\text{A.9})$$

The creation operators  $c_{\gamma,\sigma}^+$  are the hermitian adjoints of  $c_{\gamma,\sigma}$  and they can be obtained by the transposition of annihilation matrices A.5. It can be checked that the above matrices satisfy the anticommutation relations for fermionic operators:

$$\left[ c_{\gamma,\sigma}, c_{\gamma',\sigma'} \right]_+ = \left[ c_{\gamma,\sigma}^+, c_{\gamma',\sigma'}^+ \right]_+ = 0, \quad (\text{A.10})$$

and

$$\left[ c_{\gamma,\sigma}, c_{\gamma',\sigma'}^+ \right] = \delta_{\gamma,\gamma'} \delta_{\sigma,\sigma'}, \quad (\text{A.11})$$

as well as the Pauli principle:

$$\left( c_{\gamma,\sigma}^+ \right)^2 = \left( c_{\gamma,\sigma} \right)^2 = 0. \quad (\text{A.12})$$

## Appendix B. The pair Hamiltonian and its diagonalization

Having  $c_{\gamma,\sigma}$  and  $c_{\gamma,\sigma}^+$  in their explicit form, the matrices representing occupation numbers with a given spin,  $n_{\gamma,\sigma}$ , and  $z$ -component of resulting spin on the  $\gamma = a, b$  lattice site,  $S_\gamma^z$ , can be easily



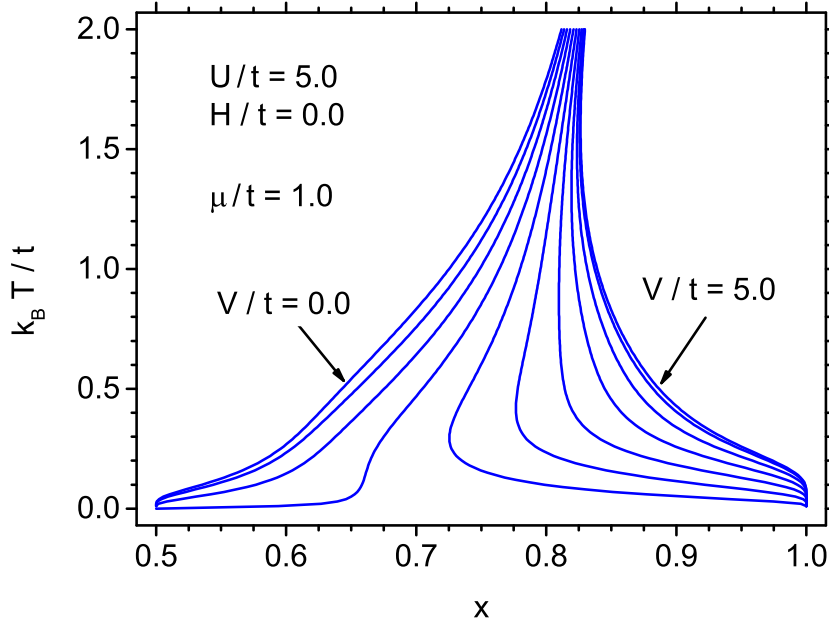


Figure 14: Isolines presenting constant electric field potentials  $V/t$ , in the coordinates  $x$  (electron concentration per atom) and  $k_B T/t$  (temperature). The curves are separated by  $|\Delta V|/t = 0.5$ . All curves correspond to the constant chemical potential  $\mu/t = 1$  and parameter  $U/t = 5$ . The magnetic field is set to zero.

found from their definitions:

$$n_{\gamma,\sigma} = c_{\gamma,\sigma}^+ c_{\gamma,\sigma}, \quad (\text{B.1})$$

and

$$S_{\gamma}^z = \frac{1}{2} (n_{\gamma,\uparrow} - n_{\gamma,\downarrow}). \quad (\text{B.2})$$

The total occupation number for given lattice site is then represented by the operator:

$$n_{\gamma} = n_{\gamma,\uparrow} + n_{\gamma,\downarrow}. \quad (\text{B.3})$$

Thus, all operators in the pair Hamiltonian (Eq. 1) can be explicitly expressed by the matrices given above. Consequently, the pair Hamiltonian can be presented as  $16 \times 16$  sparse matrix. However, in open system, we should deal with the extended Hamiltonian, containing the chemical potential term, which, after division by the hopping integral, can be presented in the dimensionless form:

$$\tilde{\mathcal{H}}_{a,b} = \frac{1}{t} [\mathcal{H}_{a,b} - \mu (n_a + n_b)] \quad (\text{B.4})$$

As a result, the extended pair Hamiltonian containing interactions with the external fields has the matrix form:

$$\tilde{\mathcal{H}}_{a,b} = \begin{pmatrix} d_1 & 0 & 0 & 0 & 0 & 0 & 0 & 0 & 0 & 0 & 0 & 0 & 0 & 0 & 0 & 0 \\ 0 & d_2 & 0 & 0 & -1 & 0 & 0 & 0 & 0 & 0 & 0 & 0 & 0 & 0 & 0 & 0 \\ 0 & 0 & d_3 & 0 & 0 & 0 & 0 & 0 & -1 & 0 & 0 & 0 & 0 & 0 & 0 & 0 \\ 0 & 0 & 0 & d_4 & 0 & 0 & 1 & 0 & 0 & -1 & 0 & 0 & 0 & 0 & 0 & 0 \\ 0 & -1 & 0 & 0 & d_5 & 0 & 0 & 0 & 0 & 0 & 0 & 0 & 0 & 0 & 0 & 0 \\ 0 & 0 & 0 & 0 & 0 & d_6 & 0 & 0 & 0 & 0 & 0 & 0 & 0 & 0 & 0 & 0 \\ 0 & 0 & 0 & 1 & 0 & 0 & d_7 & 0 & 0 & 0 & 0 & 0 & 1 & 0 & 0 & 0 \\ 0 & 0 & 0 & 0 & 0 & 0 & 0 & d_8 & 0 & 0 & 0 & 0 & 0 & 1 & 0 & 0 \\ 0 & 0 & -1 & 0 & 0 & 0 & 0 & 0 & d_9 & 0 & 0 & 0 & 0 & 0 & 0 & 0 \\ 0 & 0 & 0 & -1 & 0 & 0 & 0 & 0 & 0 & d_{10} & 0 & 0 & -1 & 0 & 0 & 0 \\ 0 & 0 & 0 & 0 & 0 & 0 & 0 & 0 & 0 & 0 & d_{11} & 0 & 0 & 0 & 0 & 0 \\ 0 & 0 & 0 & 0 & 0 & 0 & 0 & 0 & 0 & 0 & 0 & d_{12} & 0 & 0 & 1 & 0 \\ 0 & 0 & 0 & 0 & 0 & 0 & 1 & 0 & 0 & -1 & 0 & 0 & d_{13} & 0 & 0 & 0 \\ 0 & 0 & 0 & 0 & 0 & 0 & 0 & 1 & 0 & 0 & 0 & 0 & 0 & d_{14} & 0 & 0 \\ 0 & 0 & 0 & 0 & 0 & 0 & 0 & 0 & 0 & 0 & 1 & 0 & 0 & 0 & d_{15} & 0 \\ 0 & 0 & 0 & 0 & 0 & 0 & 0 & 0 & 0 & 0 & 0 & 0 & 0 & 0 & 0 & d_{16} \end{pmatrix}, \quad (\text{B.5})$$

where the diagonal elements  $d_i$  ( $i = 1, \dots, 16$ ) are listed below:

$$\begin{aligned} d_1 &= 0, \\ d_2 &= -\mu/t + V/t - H/(2t), \\ d_3 &= -\mu/t + V/t + H/(2t), \\ d_4 &= U/t - 2(\mu/t - V/t), \\ d_5 &= -\mu/t - V/t - H/(2t), \\ d_6 &= -2\mu/t - H/t, \\ d_7 &= -2\mu/t, \\ d_8 &= U/t - 3\mu/t + V/t - H/(2t), \\ d_9 &= -\mu/t - V/t + H/(2t), \\ d_{10} &= -2\mu/t, \\ d_{11} &= -2\mu/t + H/t, \\ d_{12} &= U/t - 3\mu/t + V/t + H/(2t), \\ d_{13} &= U/t - 2(\mu/t + V/t), \\ d_{14} &= U/t - 3\mu/t - V/t - H/(2t), \\ d_{15} &= U/t - 3\mu/t - V/t + H/(2t), \\ d_{16} &= 2U/t - 4\mu/t. \end{aligned} \quad (\text{B.6})$$

The extended pair Hamiltonian  $\tilde{\mathcal{H}}_{a,b}$  fulfils the eigenequation:

$$\tilde{\mathcal{H}}_{a,b} \Psi_i = E_i \Psi_i, \quad (\text{B.7})$$

where  $E_i$  are dimensionless energies and  $\Psi_i$  are the eigenvectors ( $i=1,\dots,16$ ). In general,  $\Psi_i$  can be presented as a linear combination of orthonormal basis  $\varphi_j$  ( $j=1,\dots,16$ ), i.e.,

$$\Psi_i = \sum_{j=1}^{16} C_{i,j} \varphi_j. \quad (\text{B.8})$$

In (B.8)  $\varphi_j$  are the unit vectors represented by 1-columnar, 16th-row matrices, with the only non-zero element, equal to 1, located in the  $j$ -th row.

$$\varphi_j = \begin{pmatrix} \delta_{j,1} \\ \dots \\ \delta_{j,k} \\ \dots \\ \delta_{j,16} \end{pmatrix}. \quad (\text{B.9})$$

It follows from the matrix form of  $\tilde{\mathcal{H}}_{a,b}$  that for  $i=1,6,11$ , and 16 the corresponding energies are immediately given as:

$$E_1 = d_1 \quad ; \quad E_6 = d_6 \quad ; \quad E_{11} = d_{11} \quad \text{and} \quad E_{16} = d_{16}. \quad (\text{B.10})$$

Simultaneously, corresponding eigenvectors  $\Psi_i$  have the simple form:

$$\Psi_1 = \varphi_1 \quad ; \quad \Psi_6 = \varphi_6 \quad ; \quad \Psi_{11} = \varphi_{11} \quad \text{and} \quad \Psi_{16} = \varphi_{16}, \quad (\text{B.11})$$

respectively. In turn, for the energy pairs  $(E_2, E_5)$ ,  $(E_3, E_9)$ ,  $(E_8, E_{14})$ , and  $(E_{12}, E_{15})$ , we obtain from Eq. (B.7) corresponding blocks of 2 coupled equations for the coefficients  $C_{i,j}$ , which leads to the quadratic equations for the energy. Solving these equations one obtains:

$$\begin{aligned} E_2 &= \frac{1}{2} (d_2 + d_5) - \frac{1}{2} \sqrt{(d_2 - d_5)^2 + 4} \\ E_5 &= \frac{1}{2} (d_2 + d_5) + \frac{1}{2} \sqrt{(d_2 - d_5)^2 + 4} \\ E_3 &= \frac{1}{2} (d_3 + d_9) - \frac{1}{2} \sqrt{(d_3 - d_9)^2 + 4} \\ E_9 &= \frac{1}{2} (d_3 + d_9) + \frac{1}{2} \sqrt{(d_3 - d_9)^2 + 4} \\ E_8 &= \frac{1}{2} (d_8 + d_{14}) - \frac{1}{2} \sqrt{(d_8 - d_{14})^2 + 4} \\ E_{14} &= \frac{1}{2} (d_8 + d_{14}) + \frac{1}{2} \sqrt{(d_8 - d_{14})^2 + 4} \\ E_{12} &= \frac{1}{2} (d_{12} + d_{15}) - \frac{1}{2} \sqrt{(d_{12} - d_{15})^2 + 4} \\ E_{15} &= \frac{1}{2} (d_{12} + d_{15}) + \frac{1}{2} \sqrt{(d_{12} - d_{15})^2 + 4}. \end{aligned} \quad (\text{B.12})$$

Corresponding eigenvectors have the form of:

$$\begin{aligned}
 \Psi_2 &= \frac{1}{\sqrt{1 + (d_5 - E_2)^2}} [(d_5 - E_2) \varphi_2 + \varphi_5] \\
 \Psi_5 &= \frac{1}{\sqrt{1 + (d_5 - E_5)^2}} [(d_5 - E_5) \varphi_2 + \varphi_5] \\
 \Psi_3 &= \frac{1}{\sqrt{1 + (d_9 - E_3)^2}} [(d_9 - E_3) \varphi_3 + \varphi_9] \\
 \Psi_9 &= \frac{1}{\sqrt{1 + (d_9 - E_9)^2}} [(d_9 - E_9) \varphi_3 + \varphi_9] \\
 \Psi_8 &= \frac{1}{\sqrt{1 + (d_{14} - E_8)^2}} [-(d_{14} - E_8) \varphi_8 + \varphi_{14}] \\
 \Psi_{14} &= \frac{1}{\sqrt{1 + (d_{14} - E_{14})^2}} [-(d_{14} - E_{14}) \varphi_8 + \varphi_{14}] \\
 \Psi_{12} &= \frac{1}{\sqrt{1 + (d_{15} - E_{12})^2}} [-(d_{15} - E_{12}) \varphi_{12} + \varphi_{15}] \\
 \Psi_{15} &= \frac{1}{\sqrt{1 + (d_{15} - E_{15})^2}} [-(d_{15} - E_{15}) \varphi_{12} + \varphi_{15}].
 \end{aligned} \tag{B.13}$$

Remaining four energies:  $E_4$ ,  $E_7$ ,  $E_{10}$ , and  $E_{13}$ , can be found from Eq. (B.7) as the solutions of the block of 4 coupled equations for coefficients  $C_{i,j}$ . This leads to the 4th order algebraic equation for the energy:

$$E^4 + b E^3 + c E^2 + d E + e = 0, \tag{B.14}$$

where the coefficients  $b, c, d$  and  $e$  can be presented as:

$$\begin{aligned}
 b &= -(d_4 + d_7 + d_{10} + d_{13}) \\
 c &= d_4 d_7 + d_{10} d_{13} + (d_4 + d_7)(d_{10} + d_{13}) - 4 \\
 d &= -d_4 d_7 (d_{10} + d_{13}) - d_{10} d_{13} (d_4 + d_7) + 2(d_4 + d_7 + d_{10} + d_{13}) \\
 e &= -(d_4 + d_{13})(d_7 + d_{10}) + d_4 d_7 d_{10} d_{13}.
 \end{aligned} \tag{B.15}$$

The 4th-order algebraic equation in the general form of (B.14) can be solved analytically by the methods which can be found in mathematical handbooks [66]. These quite long, but standard, methods will not be repeated here. As a result one obtains 4 analytic solutions for energies:  $E_4$ ,  $E_7$ ,  $E_{10}$ , and  $E_{13}$ , which are real and can be used for finding corresponding eigenvectors. In order to present these eigenstates  $\Psi_4$ ,  $\Psi_7$ ,  $\Psi_{10}$ , and  $\Psi_{13}$ , we define auxiliary functions:

$$\begin{aligned}
 f_4(E_i) &= \frac{d_{13} - E_i}{d_4 - E_i} \\
 f_7(E_i) &= -\frac{d_4 + d_{13} - 2E_i}{(d_4 - E_i)(d_7 - E_i)} \\
 f_{10}(E_i) &= \frac{d_4 + d_{13} - 2E_i}{(d_4 - E_i)(d_{10} - E_i)}
 \end{aligned} \tag{B.16}$$

for  $i = 4, 7, 10$  and  $13$ , and

$$F(E_i) = \frac{1}{\sqrt{1 + f_4^2(E_i) + f_7^2(E_i) + f_{10}^2(E_i)}}. \quad (\text{B.17})$$

With these functions, the eigenvectors for  $i = 4, 7, 10$  and  $13$ , can be expressed in the form of linear combination:

$$\Psi_i = F(E_i) [f_4(E_i) \varphi_4 + f_7(E_i) \varphi_7 + f_{10}(E_i) \varphi_{10} + \varphi_{13}], \quad (\text{B.18})$$

where  $\varphi_i$  are the unit vectors as defined in Eq. (B.9).

It can be checked that  $\Psi_i$  for  $i = 1, \dots, 16$ , form the orthonormal and complete vector set. Thus, the full spectrum of energies  $E_i$  and corresponding eigenvectors  $\Psi_i$  have analytically been determined for the Hubbard pair treated as an open system, whose interactions with the external fields are described by the extended dimensionless Hamiltonian  $\tilde{\mathcal{H}}_{a,b}$  (Eq. (B.4)).

## References

- [1] P. W. Anderson, New approach to the theory of superexchange interactions, Phys. Rev. 115 (1959) 2–13. doi:10.1103/PhysRev.115.2.
- [2] J. Hubbard, Electron correlations in narrow energy bands, Proceedings of the Royal Society of London A: Mathematical, Physical and Engineering Sciences 276 (1365) (1963) 238–257. doi:10.1098/rspa.1963.0204.
- [3] M. C. Gutzwiller, Effect of correlation on the ferromagnetism of transition metals, Phys. Rev. Lett. 10 (1963) 159–162. doi:10.1103/PhysRevLett.10.159.
- [4] J. Kanamori, Electron correlation and ferromagnetism of transition metals, Progress of Theoretical Physics 30 (3) (1963) 275–289. doi:10.1143/PTP.30.275.
- [5] C. C. Chen, M.-H. Huang, Field and temperature dependence of thermodynamic and correlation functions of Hubbard model, Journal of Applied Physics 50 (B3) (1979) 1761–1763. doi:10.1063/1.327211.
- [6] W.-C. Ho, J. H. Barry, Cluster-variation method applied in two-site approximation to the Hubbard model at high temperatures, Phys. Rev. B 20 (1979) 2118–2128. doi:10.1103/PhysRevB.20.2118.
- [7] S. Robaszkiewicz, R. Micnas, K. A. Chao, Thermodynamic properties of the extended Hubbard model with strong intra-atomic attraction and an arbitrary electron density, Phys. Rev. B 23 (1981) 1447–1458. doi:10.1103/PhysRevB.23.1447.
- [8] S. Robaszkiewicz, R. Micnas, K. A. Chao, Chemical potential and order parameter of extended Hubbard model with strong intra-atomic attraction, Phys. Rev. B 24 (1981) 1579–1582. doi:10.1103/PhysRevB.24.1579.
- [9] J. E. Hirsch, Renormalization-group study of the Hubbard model, Phys. Rev. B 22 (1980) 5259–5266. doi:10.1103/PhysRevB.22.5259.
- [10] J. E. Hirsch, Two-dimensional Hubbard model: Numerical simulation study, Phys. Rev. B 31 (1985) 4403–4419. doi:10.1103/PhysRevB.31.4403.
- [11] J. E. Hirsch, S. Tang, Antiferromagnetism in the two-dimensional Hubbard model, Phys. Rev. Lett. 62 (1989) 591–594. doi:10.1103/PhysRevLett.62.591.
- [12] E. H. Lieb, Two theorems on the Hubbard model, Phys. Rev. Lett. 62 (1989) 1201–1204. doi:10.1103/PhysRevLett.62.1201.
- [13] E. H. Lieb, F. Y. Wu, Absence of Mott transition in an exact solution of the short-range, one-band model in one dimension, Phys. Rev. Lett. 20 (1968) 1445–1448. doi:10.1103/PhysRevLett.20.1445.
- [14] E. H. Lieb, F. Wu, The one-dimensional Hubbard model: a reminiscence, Physica A: Statistical Mechanics and its Applications 321 (12) (2003) 1 – 27. doi:10.1016/S0378-4371(02)01785-5.
- [15] S. Sorella, E. Tosatti, Semi-metal-insulator transition of the Hubbard model in the honeycomb lattice, EPL (Europhysics Letters) 19 (8) (1992) 699. doi:10.1209/0295-5075/19/8/007.
- [16] A. Pelizzola, The half-filled Hubbard model in the pair approximation of the cluster variation method, Journal of Physics A: Mathematical and General 26 (9) (1993) 2061. doi:10.1088/0305-4470/26/9/005.

- [17] V. Janiš, D. Vollhardt, Construction of analytically tractable mean-field theories for quantum models, *Zeitschrift für Physik B Condensed Matter* 91 (3) (1993) 317–323. doi:10.1007/BF01344060.
- [18] Staudt, R., Dzierzawa, M., Muramatsu, A., Phase diagram of the three-dimensional Hubbard model at half filling, *Eur. Phys. J. B* 17 (3) (2000) 411–415. doi:10.1007/s100510070120.
- [19] N. M. R. Peres, M. A. N. Araújo, D. Bozi, Phase diagram and magnetic collective excitations of the Hubbard model for graphene sheets and layers, *Phys. Rev. B* 70 (2004) 195122. doi:10.1103/PhysRevB.70.195122.
- [20] P. R. C. Kent, M. Jarrell, T. A. Maier, T. Pruschke, Efficient calculation of the antiferromagnetic phase diagram of the three-dimensional Hubbard model, *Phys. Rev. B* 72 (2005) 060411. doi:10.1103/PhysRevB.72.060411.
- [21] T. A. Zaleski, T. K. Kopeć, Néel order in the Hubbard model within a spin-charge rotating reference frame approach: Crossover from weak to strong coupling, *Phys. Rev. B* 77 (2008) 125120. doi:10.1103/PhysRevB.77.125120.
- [22] R. Schumann, D. Zwicker, The Hubbard model extended by nearest-neighbor Coulomb and exchange interaction on a cubic cluster: rigorous and exact results, *Annalen der Physik* 522 (6) (2010) 419–439. doi:10.1002/andp.201010452.
- [23] R. Schumann, Rigorous solution of a Hubbard model extended by nearest-neighbour Coulomb and exchange interaction on a triangle and tetrahedron, *Annalen der Physik* 17 (4) (2008) 221–259. doi:10.1002/andp.200710281.
- [24] J. Čisárová, J. Strečka, Exact solution of a coupled spinelectron linear chain composed of localized Ising spins and mobile electrons, *Physics Letters A* 378 (3839) (2014) 2801 – 2807. doi:10.1016/j.physleta.2014.07.049.
- [25] H. Čenčariková, J. Strečka, M. L. Lyra, Reentrant phase transitions of a coupled spin-electron model on doubly decorated planar lattices with two or three consecutive critical points, *Journal of Magnetism and Magnetic Materials* 401 (2016) 1106 – 1122. doi:10.1016/j.jmmm.2015.11.018.
- [26] L. Gálisová, J. Strečka, Magnetic Grüneisen parameter and magnetocaloric properties of a coupled spinelectron double-tetrahedral chain, *Physics Letters A* 379 (39) (2015) 2474 – 2478. doi:10.1016/j.physleta.2015.07.007.
- [27] L. Gálisová, J. Strečka, Vigorous thermal excitations in a double-tetrahedral chain of localized Ising spins and mobile electrons mimic a temperature-driven first-order phase transition, *Phys. Rev. E* 91 (2015) 022134. doi:10.1103/PhysRevE.91.022134.
- [28] A. B. Harris, R. V. Lange, Single-particle excitations in narrow energy bands, *Phys. Rev.* 157 (1967) 295–314. doi:10.1103/PhysRev.157.295.
- [29] A. V. Silant'ev, A dimer in the extended Hubbard model, *Russian Physics Journal* 57 (11) (2015) 1491–1502. doi:10.1007/s11182-015-0406-z.
- [30] H. Hasegawa, Nonextensive thermodynamics of the two-site Hubbard model, *Physica A: Statistical Mechanics and its Applications* 351 (24) (2005) 273 – 293. doi:10.1016/j.physa.2005.01.025.
- [31] H. Hasegawa, Thermal entanglement of Hubbard dimers in the nonextensive statistics, *Physica A: Statistical Mechanics and its Applications* 390 (8) (2011) 1486 – 1503. doi:10.1016/j.physa.2010.12.033.
- [32] J. Spałek, A. Oleś, K. Chao, Thermodynamic properties of a two-site Hubbard model with orbital degeneracy, *Physica A: Statistical Mechanics and its Applications* 97 (3) (1979) 552 – 564. doi:10.1016/0378-4371(79)90095-5.
- [33] S. Longhi, G. Della Valle, V. Foglietti, Classical realization of two-site Fermi-Hubbard systems, *Phys. Rev. B* 84 (2011) 033102. doi:10.1103/PhysRevB.84.033102.
- [34] R. Juliano, A. de Arruda, L. Craco, Coexistence and competition of on-site and intersite Coulomb interactions in Mott-molecular-dimers, *Solid State Communications* 227 (2016) 51 – 55. doi:10.1016/j.ssc.2015.11.021.
- [35] M. E. Kozlov, V. A. Ivanov, K. Yakushi, Development of a two-site Hubbard model for analysis of the electron-molecular vibration coupling in organic charge-transfer salts, *Physics Letters A* 214 (3) (1996) 167 – 174. doi:10.1016/0375-9601(96)00113-2.
- [36] J. Li, C. Aron, G. Kotliar, J. E. Han, Electric-field-driven resistive switching in the dissipative Hubbard model, *Phys. Rev. Lett.* 114 (2015) 226403. doi:10.1103/PhysRevLett.114.226403.
- [37] A. V. Jura, J. K. Freericks, A. I. Lichtenstein, Long-lived nonequilibrium states in the Hubbard model with an

- electric field, Phys. Rev. B 91 (2015) 245153. doi:10.1103/PhysRevB.91.245153.
- [38] B. Alvarez-Fernández, J. A. Blanco, The Hubbard model for the hydrogen molecule, European Journal of Physics 23 (1) (2002) 11. doi:10.1088/0143-0807/23/1/302.
  - [39] R. McKenzie, A strongly correlated electron model for the layered organic superconductors kappa-(BEDT-TTF)2X, Comments on Condensed Matter Physics 18 (1998) 309.
  - [40] S. Fuchs, E. Gull, L. Pollet, E. Burovski, E. Kozik, T. Pruschke, M. Troyer, Thermodynamics of the 3D Hubbard model on approaching the Néel transition, Phys. Rev. Lett. 106 (2011) 030401. doi:10.1103/PhysRevLett.106.030401.
  - [41] G. Rohringer, A. Toschi, A. Katanin, K. Held, Critical properties of the half-filled Hubbard model in three dimensions, Phys. Rev. Lett. 107 (2011) 256402. doi:10.1103/PhysRevLett.107.256402.
  - [42] E. Kozik, E. Burovski, V. W. Scarola, M. Troyer, Néel temperature and thermodynamics of the half-filled three-dimensional Hubbard model by diagrammatic determinant monte carlo, Phys. Rev. B 87 (2013) 205102. doi:10.1103/PhysRevB.87.205102.
  - [43] N. Karchev, Quantum critical behavior in three-dimensional one-band Hubbard model at half-filling, Annals of Physics 333 (2013) 206 – 220. doi:10.1016/j.aop.2013.03.005.
  - [44] A. Yamada, Magnetic properties and Mott transition in the Hubbard model on the anisotropic triangular lattice, Phys. Rev. B 89 (2014) 195108. doi:10.1103/PhysRevB.89.195108.
  - [45] Y. Claveau, B. Arnaud, S. D. Matteo, Mean-field solution of the Hubbard model: the magnetic phase diagram, European Journal of Physics 35 (3) (2014) 035023. doi:10.1088/0143-0807/35/3/035023.
  - [46] B. S. Shastry, Exact integrability of the one-dimensional Hubbard model, Phys. Rev. Lett. 56 (1986) 2453–2455. doi:10.1103/PhysRevLett.56.2453.
  - [47] G. Su, B.-H. Zhao, M.-L. Ge, Exact solution of the one-dimensional Hubbard model in a magnetic field, Phys. Rev. B 46 (1992) 14909–14911. doi:10.1103/PhysRevB.46.14909.
  - [48] Mancini, F., Mancini, F. P., Extended Hubbard model in the presence of a magnetic field, Eur. Phys. J. B 68 (3) (2009) 341–351. doi:10.1140/epjb/e2008-00423-3.
  - [49] L. F. Tocchio, H. Feldner, F. Becca, R. Valentí, C. Gros, Spin-liquid versus spiral-order phases in the anisotropic triangular lattice, Phys. Rev. B 87 (2013) 035143. doi:10.1103/PhysRevB.87.035143.
  - [50] H. T. Dang, X. Y. Xu, K.-S. Chen, Z. Y. Meng, S. Wessel, Mott transition in the triangular lattice Hubbard model: A dynamical cluster approximation study, Phys. Rev. B 91 (2015) 155101. doi:10.1103/PhysRevB.91.155101.
  - [51] N. D. Mermin, H. Wagner, Absence of ferromagnetism or antiferromagnetism in one- or two-dimensional isotropic Heisenberg models, Phys. Rev. Lett. 17 (1966) 1133–1136. doi:10.1103/PhysRevLett.17.1133.
  - [52] A. R. W. Nolting, Quantum Theory of Magnetism, Springer-Verlag, Berlin, 2009.
  - [53] K. Dombrowsky, S. and Dichtel, Cumulant calculations of thermodynamic quantities for the Hubbard and the Emery model, Journal of Superconductivity 9 (4) (1996) 453–456. doi:10.1007/BF00727295.
  - [54] H. Feldner, Z. Y. Meng, A. Honecker, D. Cabra, S. Wessel, F. F. Assaad, Magnetism of finite graphene samples: Mean-field theory compared with exact diagonalization and quantum Monte Carlo simulations, Phys. Rev. B 81 (2010) 115416. doi:10.1103/PhysRevB.81.115416.
  - [55] K. Szalowski, Graphene nanoflakes in external electric and magnetic in-plane fields, Journal of Magnetism and Magnetic Materials 382 (2015) 318 – 327. doi:10.1016/j.jmmm.2015.01.080.
  - [56] I. Weymann, J. Barnaś, S. Krompievski, Transport through graphenelike flakes with intrinsic spin-orbit interactions, Phys. Rev. B 92 (2015) 045427. doi:10.1103/PhysRevB.92.045427.
  - [57] K. A. Chao, J. Spalek, A. M. Oleś, Kinetic exchange interaction in a narrow s-band, Journal of Physics C: Solid State Physics 10 (10) (1977) L271. doi:10.1088/0022-3719/10/10/002.
  - [58] K. Yosida, Theory of Magnetism, Springer-Verlag, Berlin, 1998.
  - [59] H. Tasaki, The Hubbard model - an introduction and selected rigorous results, Journal of Physics: Condensed Matter 10 (20) (1998) 4353. doi:10.1088/0953-8984/10/20/004.
  - [60] R. Micnas, J. Ranninger, S. Robaszkiewicz, Superconductivity in narrow-band systems with local nonretarded attractive interactions, Rev. Mod. Phys. 62 (1990) 113–171. doi:10.1103/RevModPhys.62.113.
  - [61] A. Georges, G. Kotliar, W. Krauth, M. J. Rozenberg, Dynamical mean-field theory of strongly correlated fermion systems and the limit of infinite dimensions, Rev. Mod. Phys. 68 (1996) 13–125.

- doi:10.1103/RevModPhys.68.13.
- [62] D. Hirschmeier, H. Hafermann, E. Gull, A. I. Lichtenstein, A. E. Antipov, Mechanisms of finite-temperature magnetism in the three-dimensional Hubbard model, Phys. Rev. B 92 (2015) 144409. doi:10.1103/PhysRevB.92.144409.
- [63] A. Mielke, The Hubbard model and its properties, in: P. C. E. Pavarini, E. Koch (Ed.), Many-Body Physics: From Kondo to Hubbard, Modeling and Simulation, Vol. 5, Forschungszentrum Jülich, 2015.
- [64] Mathematica, Version 8.0.4, Wolfram Research, Inc., Champaign, IL, 2010.
- [65] M. Suffczyński, Electrons in Solids (Monographs in Physics, Vol. 1), Ossolineum, Wrocław, 1985.
- [66] Solutions of quartic equations, in: M. Abramovitz, I. A. Stegun (Eds.), Handbook of Mathematical Functions with Formulas, Graphs, and Mathematical Tables, New York: Dover, 1972, Ch. 3.8.3.